RESEARCH ARTICLE

BATTERY ENERGY WILEY

Porous ZnP matrix for long-lifespan and dendrite-free Zn metal anodes

Xinyue Lei[1] | Zhipeng Ma[1,2] | Lei Bai[1] | Lei Wang[1] | Yali Ding[1] | Shenglu Song[1] | Ailing Song[1,2] | Haifeng Dong[1] | Hao Tian[3] | Huajun Tian[4] | Xiangtong Meng[5] | Hao Liu[3] | Bing Sun[3] | Guangjie Shao[1,2] | Guoxiu Wang[3]

[1]Hebei Key Laboratory of Applied Chemistry, College of Environmental and Chemical Engineering, Yanshan University, Qinhuangdao, China

[2]State Key Laboratory of Metastable Materials Science and Technology, Yanshan University, Qinhuangdao, China

[3]Centre for Clean Energy Technology, School of Mathematical and Physical Sciences, Faculty of Science, University of Technology Sydney, Ultimo, New South Wales, Australia

[4]Key Laboratory of Power Station Energy Transfer Conversion and System of Ministry of Education, School of Energy Power and Mechanical Engineering, North China Electric Power University, Beijing, China

[5]State Key Laboratory of Organic-Inorganic Composites, College of Chemical Engineering, Beijing University of Chemical Technology, Beijing, China

Correspondence
Zhipeng Ma, Ailing Song, and Haifeng Dong, Hebei Key Laboratory of Applied Chemistry, College of Environmental and Chemical Engineering, Yanshan University, Qinhuangdao 066004, China.
Email: mazp@ysu.edu.cn, ailing.song@ysu.edu.cn and hfdong@ysu.edu.cn

Hao Tian and Bing Sun, Centre for Clean Energy Technology, School of Mathematical and Physical Sciences, Faculty of Science, University of Technology Sydney, Broadway, NSW 2007, Australia.
Email: hao.tian@uts.edu.au and bing.sun@uts.edu.au

Abstract

The reversibility of Zn plating/stripping during cycling is adversely affected by dendritic growth, electrochemical corrosion, surface passivation, and hydrogen generation on the Zn anodes for rechargeable aqueous zinc ion batteries (ZIBs). Herein, through an ordinary anodic etching process, a uniform porous ZnP matrix protective layer was created on the Zn foil (Zn@ZnP). The large and accessible specific surface area of the prepared Zn@ZnP can facilitate contact with the electrolyte, accelerating the migration and enhancing the desolvation of Zn^{2+}, effectively enhancing the Zn deposition kinetics. According to studies from scanning electron microscopy (SEM) and multiscale optical microscopy, the Zn@ZnP electrode effectively inhibits the growth of dendrites with excellent Zn plating/stripping reversibility. In consequence, the symmetric cell with the Zn@ZnP electrodes displays a long-term cycle life of over 1260 h at 10 mA cm^{-2}. The full cell, consisting of Zn@ZnP anodes and MnO_2-based cathode, demonstrated a high discharge capacity of 145 mAh g^{-1} after cycling 500 times at the current density of 1000 mA g^{-1}. A scalable method for designing a homogeneous anode protection layer enables dendrite-free zinc metal anodes, paving the way for interface modification of other metal anodes.

1 | INTRODUCTION

Rechargeable aqueous zinc ion batteries (ZIBs) have garnered worldwide attention for their cost-effectiveness as well as the safety associated with Zn metal. With a relatively low redox potential of 0.76 V compared to standard hydrogen electrodes (SHE), ZIBs boast a high theoretical mass-specific capacity of 820 mAh g^{-1} and volume-specific capacity of 5855 mAh cm^{-3}.[1–4] However, Zn metal is chemically reactive and thermodynamically unstable in weak acid electrolytes, leading to the generation of by-products.[5–7] Additionally, the uneven distribution of electric fields over the Zn metal anode surface leads to irregular Zn deposition, which eventually triggers the growth of dendrites to penetrate the separators and lead to short circuits.[8,9] Finally, it is impractical to utilize ZIBs given their low Coulombic efficiency (CE) and short lifespan.[10] Therefore, establishing a dendrite-free Zn anode is crucial to ensuring the optimal performance of ZIBs.[11–13]

To address the aforementioned problems, a variety of ways have been sought to enhance the stability as well as facilitate uniform deposition of Zn metal anodes, including electrolyte optimization,[14–16] separator modifications[17,18] and electrode/electrolyte interface engineering.[19–26] The construction of an artificial interface layer over Zn metal has been considered one of the most encouraging strategies for electrode/electrolyte interface engineering.[27] By isolating the Zn foil surface from the electrolyte and creating an artificial protective layer, we can minimize side reactions and inhibit Zn dendrite growth.[28,29] To create the artificial protection layer, there are two primary methods: (1) ex situ construction of an ionic conductive layer on the Zn anode surface; (2) in situ construction of a protective layer over the Zn anode surface. Ex situ coating Zn foil with a montmorillonite layer can accelerate Zn^{2+} diffusion, reduce corrosion and passivation, and inhibit Zn dendrite growth.[30,31] For instance, an amorphous metal–organic framework (MOF) of ATMP-Zr has been used to prepare an artificial protective surface over the Zn metal anode by scraping strategy.[32] Isolating the metal substrate from the electrolyte can prevent side reactions and promote uniform Zn deposition. Except for MOFs,[33] more nanomaterials and polymers have been applied to construct artificial protective layers, such as nano-HfO$_2$,[34] TiO$_2$/polyvinylidene fluoride[35], and poly(vinyl butyral).[28] However, during prolonged cycling at higher current densities, the ex situ physical coating may suffer from problems such as cracking and exfoliation, resulting in direct contact between the electrolyte and the freshly exposed Zn metal and continuous side reactions.[36]

In contrast, the in situ formed protective layers with homogeneous morphologies show strong bonding affinity with the Zn metal. It significantly enhances the structural integrity of the protective layer during long-term cycling, contributing to excellent battery performance.[37–39] For instance, MOF-based compounds, UiO-66-(COOH)$_2$ with carboxyl functionalized pores, were used to construct a multifunctional ion-conducting interface for the Zn metal anode. This interface effectively facilitates the desolvation process of hydrated Zn^{2+} and the diffusion of Zn^{2+} near the surface of Zn anodes, thereby inhibiting side reactions and facilitating even Zn deposition.[40] Alloy compounds, such as ZnTe,[41] ZnF$_2$-Ag,[8] nanoporous ZnO,[42] and S/MX@ZnS, were also in-situ built over the Zn anode surface as protective layers.[19] In addition, ZnP alloy can significantly accelerate the desolvation rate of Zn^{2+}, facilitating zinc deposition. The incorporated P can boost the Zn^{2+} ion transfer rate and reduce the energy barrier of electrochemical reaction on the Zn plating/stripping process, effectively improving the cycling stability of Zn anodes.[43,44] However, the thickness and uniformity of the ZnP protective layer obtained via the electrodeposition method may be difficult to control.

Herein, inspired by the excellent protection of ZnP alloy materials, a highly reversible Zn metal anode was designed through the in situ growth of an artificial protective layer with a three-dimensional (3D) interconnected ZnP alloy structure over a Zn foil surface (Zn@ZnP) by a controllable and efficient anodic etching method. The anodic etching method also chemically reconstructs the zinc foil while preparing the ZnP layer, which further removes the zinc oxide present on the surface of the zinc foil. Due to the 3D porous structure, the zinc anode's specific surface area is also increased. The broad specific surface area provided by the 3D structure provides sufficient zinc deposition sites for the battery cycle and effectively avoids the generation of zinc

dendrites.[43,45–48] According to the analysis of the multi-scale in situ and ex situ microscopy observations, the prepared Zn@ZnP anodes facilitate homogeneous Zn deposition, which benefits from accelerated Zn^{2+} migration rate and enhanced Zn^{2+} desolvation kinetics of the ZnP protective layers. The symmetric cell can operate for 2000 h at $1\,mA\,cm^{-2}$, according to the electrochemical testing findings, and it has a stable voltage hysteresis. After increasing the current density to $10\,mA\,cm^{-2}$, the symmetric cell serves over 1260 h. With the aluminum intercalated δ-MnO_2 on a reduced graphene oxide nanosheet (AMGO) cathode, the assembled full cell shows an outstanding discharge capacity of $145\,mAh\,g^{-1}$ after 500 cycles at $1000\,mA\,g^{-1}$.

2 | RESULTS AND DISCUSSION

The Zn deposition behaviors on pristine Zn and Zn@ZnP anodes are illustrated in Figure 1. Figure 1A shows that the appearance of small protrusions is due to the uneven deposition and gradual accumulation of zinc on the bare zinc surface. These protrusions eventually form dendrites. In addition, the contact with the aqueous electrolyte generates H_2 in a weak acid electrolyte and produces by-products (i.e., $Zn(OH)_2$ and $Zn_4SO_4(OH)_6 \cdot H_2O$), severely corroding the Zn anode inexorably. Those by-products are deposited on the zinc surface and generate a passivating layer that significantly increases the charge transfer resistance of Zn-ion batteries. In contrast, Zn foil with a protective layer, porous interconnected ZnP matrix, can promote uniform Zn deposition and effectively inhibit side reactions during reduplicative plating/stripping of Zn^{2+}/Zn (Figure 1B). By enhancing interaction with the electrolyte, accelerating Zn^{2+} diffusion, and enhancing Zn^{2+} desolvation, the protective surface on the Zn anodes increases Zn deposition kinetics and facilitates homogenous Zn deposition.

The field emission scanning electron microscopy (FESEM) image displayed the Zn surface's morphology changes before and after treatment in different conditions. The surface of the pure Zn foil is relatively smooth (Figure 2A). After anodic etching treatment in 0.1 M NaH_2PO_2 solution, the pristine Zn surface presents an uneven and porous structure (Figure 2B). As the concentration of the solution increases to 0.2 M, the Zn surface presents a uniform 3D structure with a porous skeleton (Figure 2C). Some agglomerates appear on the Zn foil after being treated in 0.6 M NaH_2PO_2 solution (Figure 2D). When the concentration of the solution reaches 1.0 M, a serious agglomeration phenomenon appears on the Zn foil, resulting in uneven surface morphology (Figure 2E). The composition of materials and their distribution were investigated using energy dispersive spectroscopy (EDS). The signals of the Zn element and P element are uniformly distributed on the Zn surface as shown in Figure 2F,G. Further study using transmission electron microscopy (TEM) was carried out to demonstrate the presence of an interconnected ZnP matrix in Supporting Information: Figure S1. X-ray
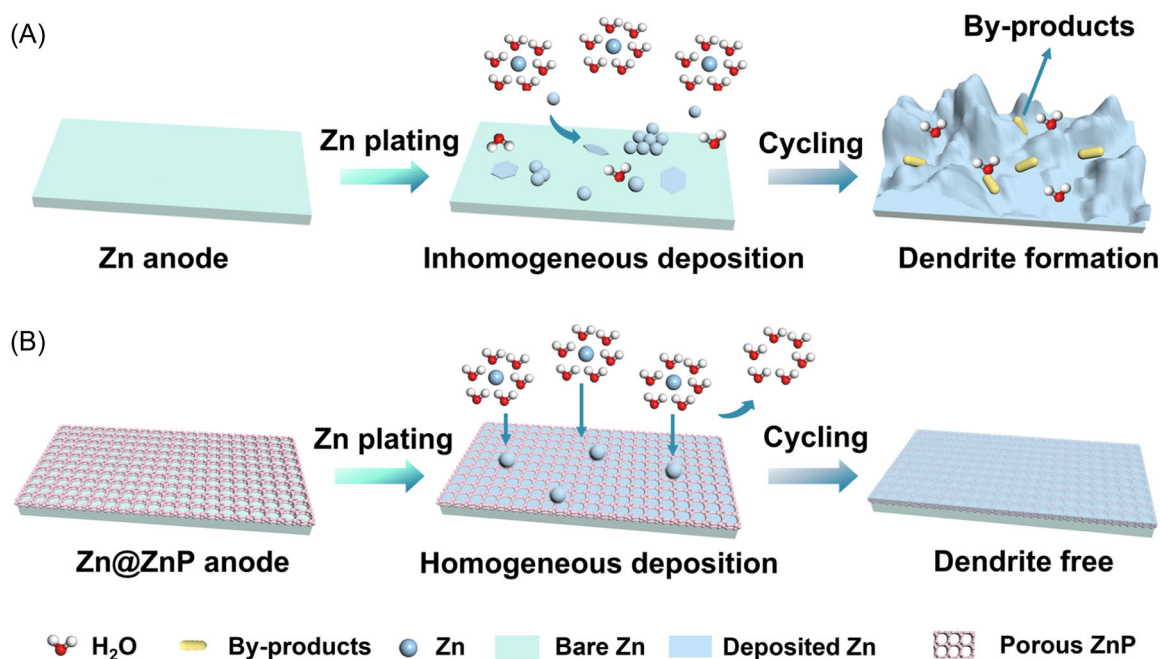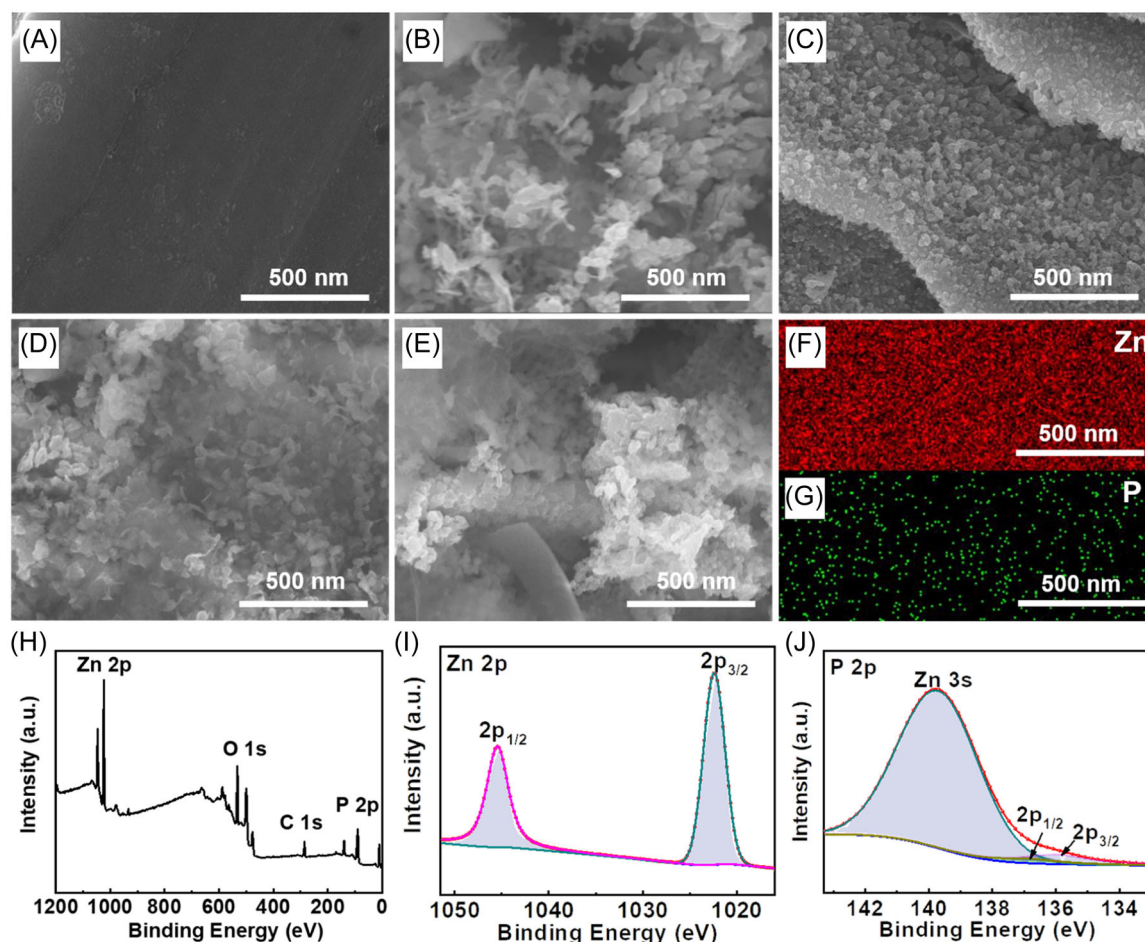

FIGURE 1 Schematic illustration of Zn deposition processes on different substrates. (A) pristine Zn foil and (B) Zn@ZnP foil.

FIGURE 2 (A) scanning electron microscopy (SEM) image of the pristine Zn foil. (B–E) SEM images of the obtained Zn@ZnP foils after the anodic etching treatment in NaH_2PO_2 solutions with different concentrations. (B) 0.1 M, (C) 0.2 M, (D) 0.6 M, and (E) 1 M. (F, G) The energy dispersive spectroscopy element analysis of Zn@ZnP. (H) X-ray photoelectron spectroscopy (XPS) survey spectrum of Zn@ZnP. (I, J) The corresponding high-resolution XPS spectra of (I) Zn 2p, and P 2p.

photoelectron spectroscopy (XPS) confirmed the element content of Zn@ZnP (Figure 2H–J). The XPS spectra of the Zn@ZnP anode revealed a typical Zn 2p diffraction peak (Figure 2I). The existence of P in the protective layer may be shown by the P 2p signal located at 134.5 eV in Figure 2J.[43] The good wettability of electrodes in electrolytes could promote the migration of Zn^{2+} at the surface of the electrodes and facilitate uniform Zn deposition. To demonstrate the wettability of pristine Zn anode and Zn@ZnP anode in 2 M $ZnSO_4$ aqueous electrolytes, contact angle testing was carried out (Supporting Information: Figure S2). The Zn@ZnP anode has a contact angle value of 50°, which is significantly different from that of the pristine Zn anode (97°), illustrating the enhanced wettability of the Zn@ZnP anode in aqueous electrolytes.

The electrochemical performances of Zn anodes were first tested by cyclic voltammetry (CV). Figure 3A shows that the CV curves of the pristine Zn anode and the

Zn@ZnP anode demonstrate analogous redox peaks, revealing the excellent reaction kinetics of Zn deposition on the Zn@ZnP anode. The $ZnSO_4$ electrolyte's weak acidity causes complicated side reactions on the electrode intersurface,[49] which triggers the hydrogen generation and raises the electrolyte's pH level.[37,38,50] We tested the stability of various electrodes by soaking them in 2 M $ZnSO_4$ solution for 3 days. The electrodes were then removed from the electrolyte solution and tested by X-ray diffraction (XRD) measurement (Supporting Information: Figure S3). The intensity and width of the prominent peaks of the Zn matrix become stronger and broader, especially (002), (101), and (102) at 36°, 39°, and 54°, respectively, illustrating that the additional P atoms cause these crystal faces to be exposed on the zinc foil. In addition, the XRD pattern of the pristine Zn foil shows diffraction peaks at 12°, 21°, and 25°, corresponding to the (001), (002), and (111) crystal planes of the $Zn_4SO_4(OH)_6 \cdot xH_2O$ (PDF#39-0690). It demonstrates that
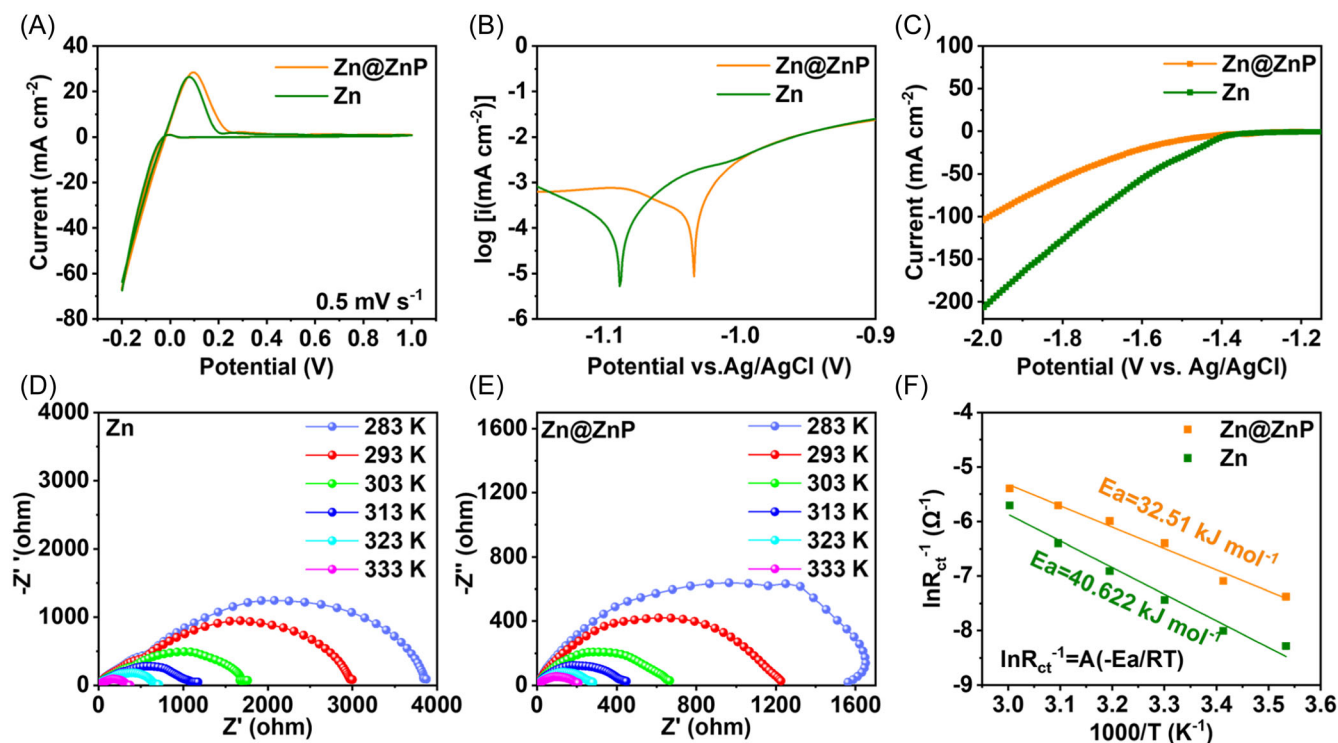
FIGURE 3 (A) Cyclic voltammetry curves of Zn and Zn@ZnP. (B) Linear polarization curves of the corrosion test of Zn and Zn@ZnP in 1 M Na_2SO_4 solution. (C) Linear sweep voltammetry curves of the hydrogen evolution test of Zn and Zn@ZnP in 1 M Na_2SO_4 solution. (D, E) Electrochemical impedance spectroscopy results were obtained at different temperatures. (F) Corresponding Arrhenius plots and comparison of activation energies of Zn and Zn@ZnP electrodes.

pristine Zn foil is prone to corrosion in contact with the $ZnSO_4$ electrolyte. In contrast, the XRD pattern of Zn@ZnP anode shows much weaker diffraction peaks corresponding to $Zn_4SO_4(OH)_6 \cdot xH_2O$, indicating that the ZnP layer effectively inhibits the corrosion reaction against aqueous electrolyte. The linear polarization experiment and linear sweep voltammetry (LSV) curves also confirmed the excellent protective effect of the ZnP layer on pristine Zn foil in 1 M Na_2SO_4 solution. In this process, Na_2SO_4 was chosen as the electrolyte instead of $ZnSO_4$ because zinc ions will be reduced in preference to hydrogen ions in the hydrogen evolution reaction, thus influencing the experimental results. As shown in the linear polarization curves in Figure 3B, the corrosion potential of the Zn@ZnP electrode (−1.032 V vs. Ag/AgCl) is positively shifted by 58 mV compared with the Zn foil (−1.090 V vs. Ag/AgCl), indicating that the ZnP protective layer can be much efficiently able to prevent the corrosion and the hydrogen evolution.[51,52] LSVs were verified over a wide voltage range (−1.2 to −2.0 V vs. Ag/AgCl) in 1 M Na_2SO_4 solution (Figure 3C). The fact that Zn@ZnP exhibits a much lower current density for hydrogen evolution than pristine Zn foil suggests that Zn foil protected by ZnP can significantly slow down hydrogen evolution.

The impact of the ZnP protective layer on Zn^{2+} migration was investigated in symmetrical cells, and the activation energy (E_a) reflecting the interface diffusion barrier of Zn^{2+} was evaluated through resistance response in the temperature range of 10–60°C, according to the Arrhenius formula.[53] The improvement of the desolvation process on the Zn@ZnP electrode at different temperatures was validated by the apparent Ea from electrochemical impedance spectroscopy (EIS) (Figure 3D,E). Obviously, the R_{ct} of pristine Zn electrodes is higher than that of Zn@ZnP electrodes at a variety of temperatures. The activation energy of the Zn@ZnP electrode is calculated to be 32.51 kJ mol⁻¹, which is much lower than that of the pristine Zn electrode (40.622 kJ mol⁻¹) (Figure 3F). The low activation energy accelerates the desolvation process of solvated Zn^{2+}, which promotes the reaction kinetic of Zn deposition.

To evaluate the cycle stability of the electrodes, symmetrical cells were constructed and tested under various current densities and capacity limitations. The symmetric cells' rate performances were tested with a capacity limitation of 2 mAh cm⁻² (Figure 4A). At the current density of 10 mA cm⁻², the voltage curve of the cell with the Zn electrodes started to fluctuate abnormally. With an increase in current density, the voltage
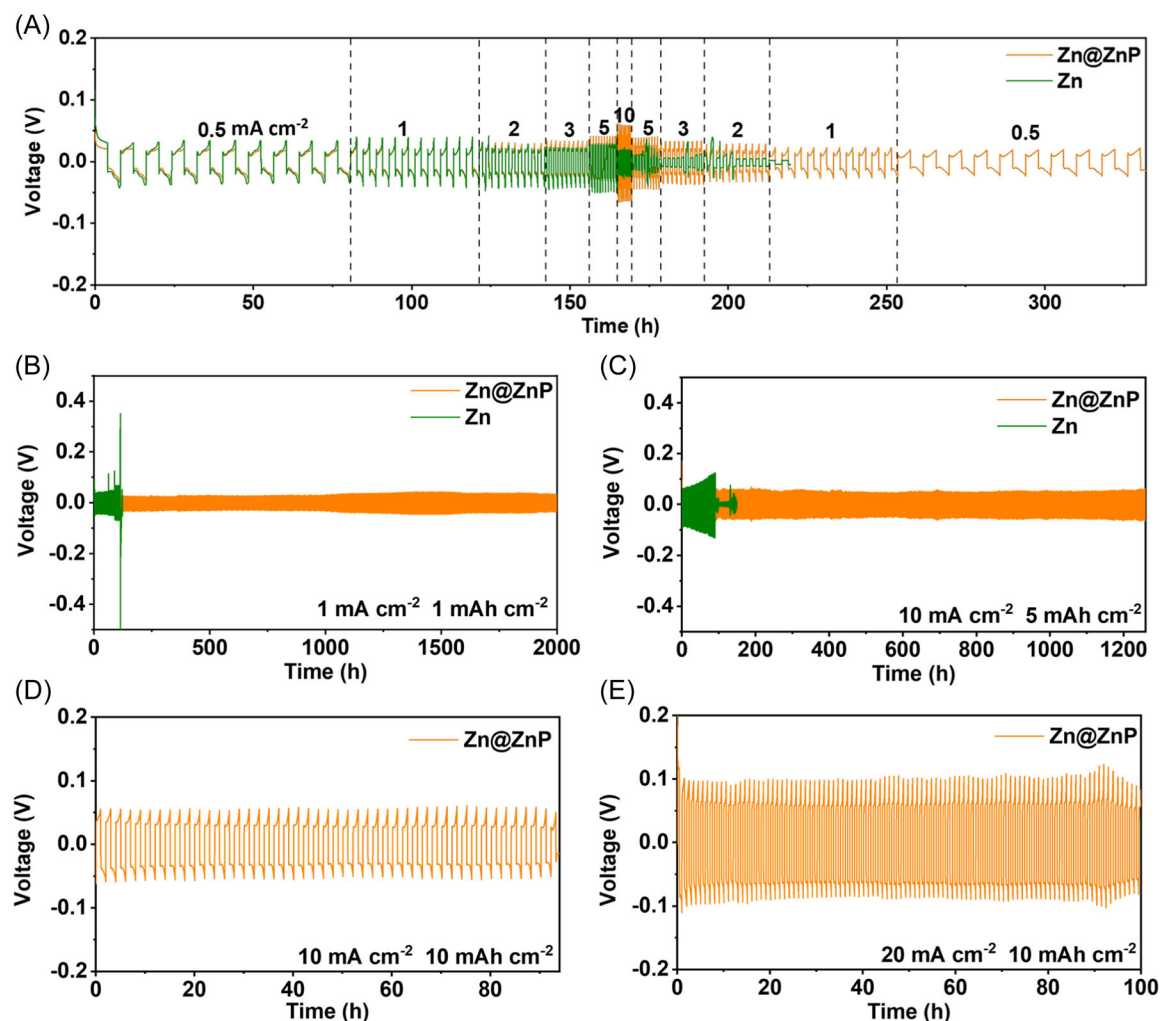
FIGURE 4 (A) The rate performance of symmetrical cells using pristine Zn electrodes or Zn@ZnP electrodes. (B–E) Long-term cycling performance of symmetrical cells using pristine Zn electrodes or Zn@ZnP electrodes at different current densities and capacity limitations. (B) 1 mA cm^{-2}, 1 mAh cm^{-2}; (C) 10 mA cm^{-2}, 5 mAh cm^{-2}; (D) 10 mA cm^{-2}, 10 mAh cm^{-2}; and (E) 20 mA cm^{-2}, 10 mAh cm^{-2}.

hysteresis of the cell with Zn@ZnP electrodes steadily grew. The Zn@ZnP electrode-equipped cell maintained stable cycling when the current density was decreased to 0.5 mA cm^{-2}. The rate performance demonstrated that the plating/stripping kinetics of the Zn@ZnP electrode had been significantly improved. As shown in Figure 4B, the electrochemical performance of Zn‖Zn and Zn@ZnP‖Zn@ZnP were compared at 1 mA cm^{-2} and a capacity limitation of 1 mAh cm^{-2}. The voltage–time curve fluctuated greatly for the cell with pristine Zn electrodes after 150 h cycling due to the dendrite growth on the surface of the Zn foil. In contrast, the cell with Zn@ZnP electrodes showed significantly improved cycling stability up to 2000 h. Once the current density reached 10 mA cm^{-2} (Figure 4C), the cell with Zn@ZnP electrodes was able to cycle steadily for 1260 h with stable plating/stripping potentials, whereas the cell with pristine Zn electrodes failed at 150 h. To further

determine the cycling stability of the Zn@ZnP electrodes at high current densities, the capacity limitation was fixed to 10 mAh cm^{-2}. At the current densities of 10 and 20 mA cm^{-2}, the cells with Zn@ZnP electrodes even cycled steadily for 95 and 100 h with low voltage hysteresis (Figure 4D,E). In addition, the cells with Zn@ZnP electrodes are more stable than the cells with pristine Zn anodes when charged and discharged at different current densities (Supporting Information: Figure S4). This indicates that the ZnP protective layer can regulate Zn^{2+} flux, inhibit the formation of dendrites, and suppress secondary processes. Additionally, varied concentrations of NaH$_2$PO$_2$ electrolytes were used to assess the electrochemical performance of Zn@ZnP electrodes. As shown in Supporting Information: Figure S5, the symmetric cells with Zn@ZnP electrode demonstrated the best cycling performance (2000 h) in 0.2 M NaH$_2$PO$_2$ electrolyte at 0.5 mA cm^{-2} and a capacity

limitation of 0.5 mAh cm^{-2}, further revealing the excellent protective effects of ZnP layer on Zn metal anodes. We performed XRD tests on the electrode after 100 cycles to confirm the stability of the protective ZnP layer (Supporting Information: Figure S6). No apparent changes in the XRD patterns except the appearance of a small amount of ZnP$_2$.

To investigate the electrochemical protection mechanism of a ZnP protective layer in the ZnSO$_4$ electrolyte system, ex situ and in situ observations combined with electrical analysis were conducted. Ex situ scanning electron microscopy (SEM) was utilized to observe the morphology evolutions during Zn deposition on both pristine Zn anodes and Zn@ZnP anodes. Figure 5A–C show the morphology evolution of pristine Zn under various deposition times in 2 M ZnSO$_4$ electrolyte with 1 mA cm^{-2}. With a plating capacity of 1 mAh cm^{-2}, pristine Zn foil showed a rough surface with lots of dendrites (Figure 5A). One of the major reasons for dendritic growth is the accumulation of local charge caused by the uneven deposition of Zn^{2+}, which leads to the creation of dendrites.[42,54] The Zn dendrites kept accumulating when the deposition reached 2 mAh cm^{-2} (Figure 5B). After the deposition capacity increased to 5 mAh cm^{-2}, the Zn anode surface was covered with dense hexagonal sheets (Figure 5C). With the increase in deposition time, dendrite growth becomes increasingly irregular, eventually leading to cell failure. In addition, the sharp dendrites with high surface areas on Zn foil further promote the side reactions with the electrolyte.[28] In contrast, the Zn@ZnP anode with
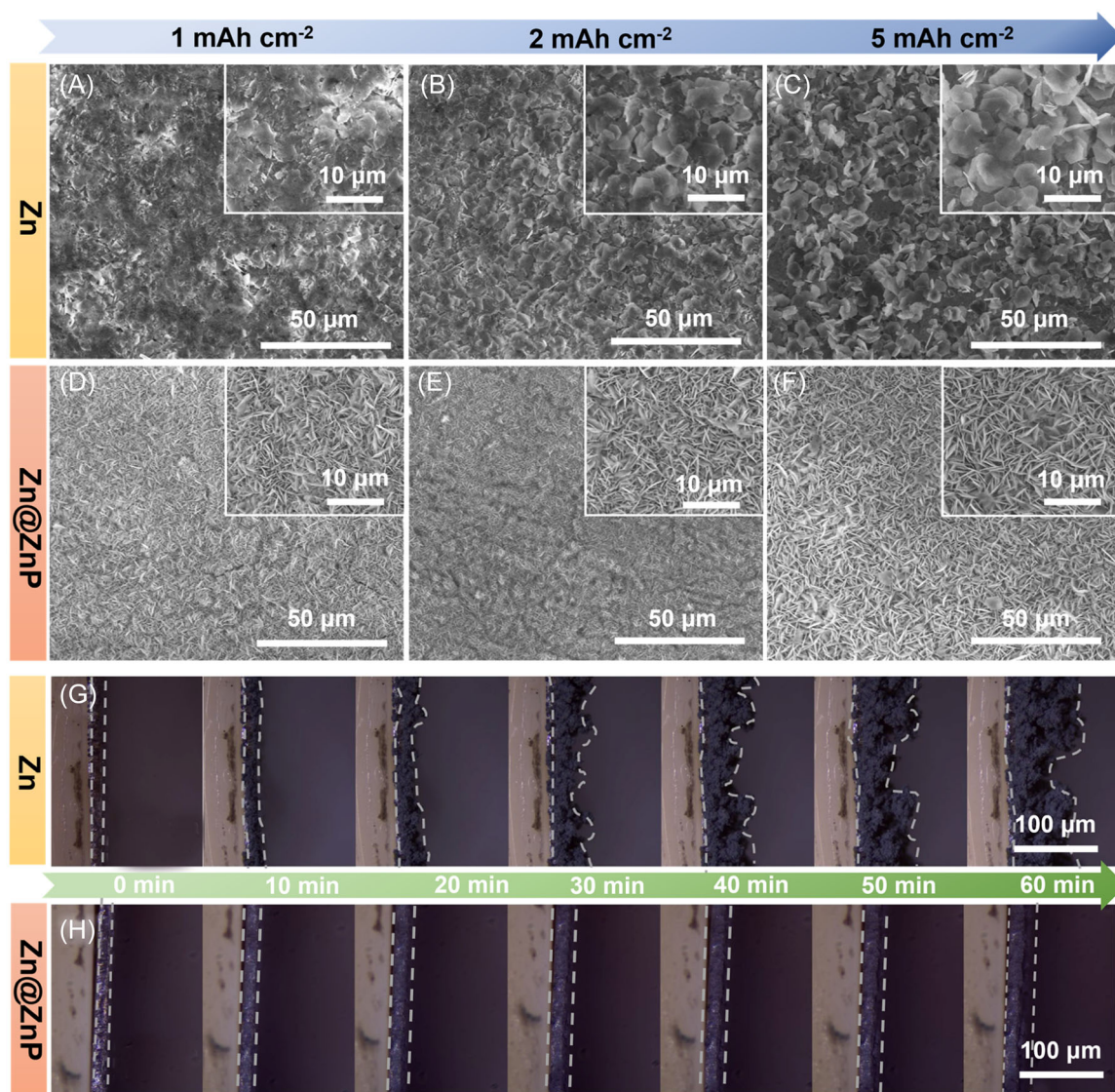

FIGURE 5 (A–F) scanning electron microscopy (SEM) images of the morphology evolution of (A–C) pristine Zn and (D–F) Zn@ZnP anodes at different capacity limitations at the current density of 1 mA cm^{-2}. The insets are the corresponding high-resolution SEM images. (G, H) In situ optical observation of the Zn plating on (G) pristine Zn anodes and (H) Zn@ZnP anode.

uniform Zn deposition was observed at different capacity limitations (Figure 5D–F). The stable variation of the Zn@ZnP surface indicated that the ZnP protective layer could uniform the nucleation and deposition of Zn, showing an excellent capability to inhibit dendrite growth. The anode surface has a flat and smooth surface due to the uniform distribution of the electric field, which also ensures consistent Zn^{2+} deposition.

Based on the above results, symmetrical cells assembled with 2 M $ZnSO_4$ electrolyte were subjected to conduct in situ optical microscopy to observe the Zn deposition process in real time. In Figure 5G, many irregular protrusions appeared on the Zn foil surface after 60 min. The protrusions gradually accumulated to form dendrites along with the deposition time.[23,55,56] The Zn@ZnP anode, however, maintained a flat and smooth surface throughout the deposition process (Figure 5H). The outcomes further demonstrated that the artificial ZnP layers can functionally inhibit dendrite growth and improve ZIBs' cycling stability.

The full cells were used to further assess the electrochemical performance of Zn@ZnP anodes and pristine Zn anodes in 2 M $ZnSO_4$ and 0.1 M $MnSO_4$ electrolytes. The aluminum intercalated δ-MnO_2 on reduced graphene oxide nanosheet (AMGO) was used as the cathode material. Supporting Information: Figures S7 and S8 show the XRD, SEM, and TEM characteristics of AMGO cathode materials. The CV curve of the Zn@ZnP-based cell shows higher redox peaks compared to the Zn-based cell, which indicates the improved electrochemical activity of the Zn@ZnP anode (Figure 6A). In addition, the Zn@ZnP-based cell exhibits a significantly lower impedance than that of the pristine Zn anode, indicating a significant decrease in charge transfer resistance during the charging and discharging operations (Figure 6B).

Gradient current densities were employed to evaluate the rate capability of the assembled full cells (Figure 6C). Under the same current densities, the cell with a Zn@ZnP anode consistently showed higher discharge-specific capacities than the cell with a pristine Zn anode. Supporting Information: Figure S9 and Figure 6D show the corresponding charge/discharge voltage profiles of full cells with the gradient current densities from 100 to 2000 mA g^{-1}. With the increase of the current density, the discharge capacity of the cell with pristine Zn anode demonstrated quick fading from 256 mAh g^{-1} at 100 mA g^{-1} to 125 mAh g^{-1} at 2000 mA g^{-1}. On the contrary, as shown in Figure 6D, compared to the pristine Zn-based cell, the Zn@ZnP-based cell achieved an improved capacity of 270 mAh g^{-1} at 100 mA g^{-1}. The discharge-specific capacity of the Zn@ZnP-based cell is 15 mAh g^{-1} at 2000 mA g^{-1}. The charge–discharge voltage curve comparison demonstrates that the Zn@ZnP anode has good reversibility and can facilitate the transfer of Zn^{2+}. At the current density of
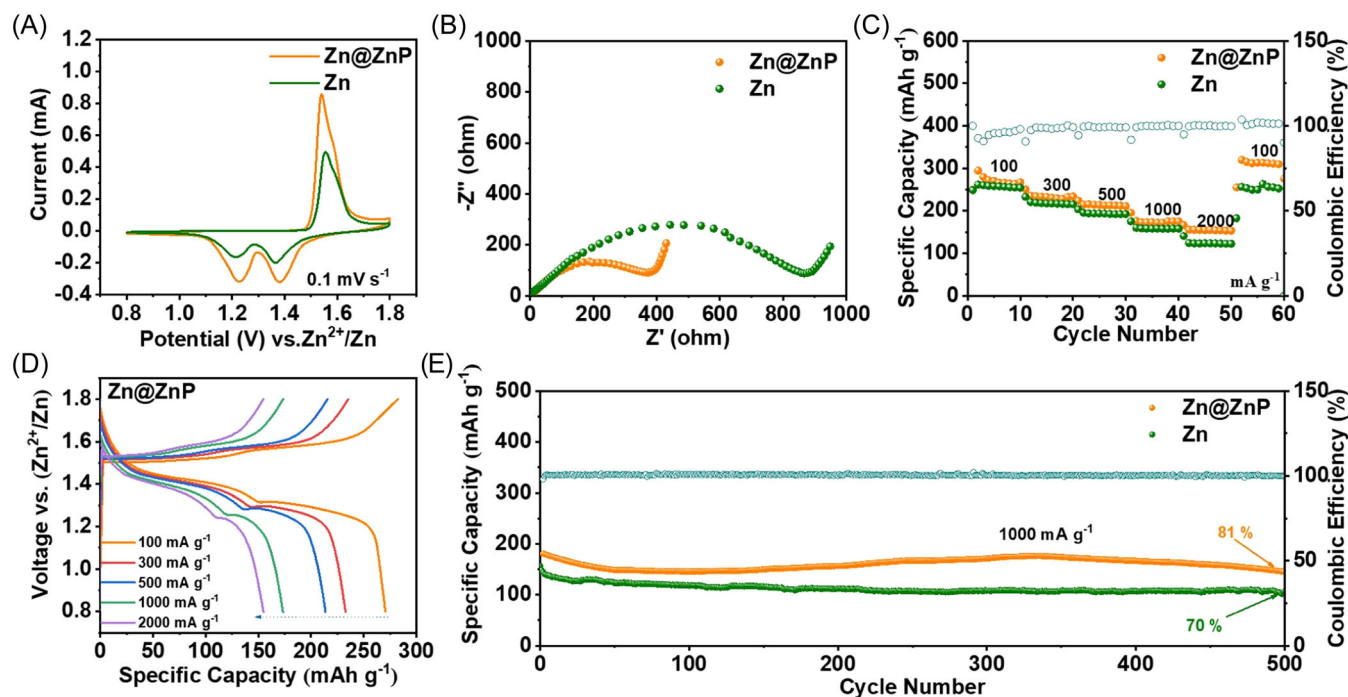

FIGURE 6 Electrochemical properties of full cells with pristine Zn anodes and Zn@ZnP anodes. (A) The cyclic voltammetry curves at the scan rate of 0.1 mV s^{-1}. (B) Electrochemical impedance spectroscopy results. (C) Rate performance. (D) The corresponding charge-discharge curves of the zinc ion battery with the Zn@ZnP anode. (E) Long-term cycling performance at the current density of 1000 mA g^{-1}.

$1000\,\text{mA g}^{-1}$, the full cell with the Zn@ZnP anode and AMGO cathode can maintain a discharge capacity of $145\,\text{mAh g}^{-1}$ after 500 cycles with a high-capacity retention of 81%, demonstrating superior stability as shown in Figure 6E. However, the full cell with Zn anode and AMGO cathode only achieved capacity retention of 70% after 500 cycles. Therefore, it can be concluded that Zn@ZnP anode has excellent stability and the ability to inhibit dendrite growth.

3 | CONCLUSION

In summary, an in situ construction of a uniform ZnP protective layer over the Zn anode surface was accomplished using a controlled anodic etching strategy. The anodic corrosion and hydrogen evolution were efficiently suppressed by the Zn@ZnP electrode, and Zn deposition kinetics were encouraged to potentially lessen polarization during cycling. In addition, the unique porous ZnP layer effectively induced even Zn deposition, thereby suppressing dendrite growth. Furthermore, in symmetric cells, the Zn@ZnP electrodes show excellent rate performance and cycling stability. With low voltage hysteresis at $1\,\text{mA cm}^{-2}$, the cell with Zn@ZnP electrodes has a stable cycle life of more than 2000 h. The symmetrical cell continued to run in a steady cycle of plating/stripping for more than 1260 h even at $10\,\text{mA cm}^{-2}$. In addition, the full cells assembled with Zn@ZnP anodes and AMGO cathodes showed outstanding cycling stability with a discharge capacity of $145\,\text{mAh g}^{-1}$ after 500 cycles at $1000\,\text{mA g}^{-1}$. The ZnP protective layer prepared by a simple anodic etching method offers a distinctive viewpoint on the protection of the Zn anode as well as a novel concept for the ZIBs interface protective layer.

CONFLICT OF INTEREST STATEMENT
The authors declare no conflict of interest.

DATA AVAILABILITY STATEMENT
Data that support the findings of this study are available from the corresponding author upon reasonable request.

ORCID
Bing Sun https://orcid.org/0000-0002-4365-486X

REFERENCES
1. Meng C, He W, Jiang L, et al. Ultra-stable aqueous zinc batteries enabled by β-cyclodextrin: preferred zinc deposition and suppressed parasitic reactions. *Adv Funct Mater.* 2022;32:2207732.
2. Wang P, Liang S, Chen C, et al. Spontaneous construction of nucleophilic carbonyl-containing interphase toward ultra-stable zinc-metal anodes. *Adv Mater.* 2022;34:2202733.
3. Yang Q, Li Q, Liu Z, et al. Dendrites in Zn-based batteries. *Adv Mater.* 2020;32:2001854.
4. Zhao Q, Liu W, Chen Y, Chen L. Ultra-stable Zn metal batteries with dendrite-free Cu-Sn alloy induced high-quality composite Zn mesh. *Chem Eng J.* 2022;450:137979.
5. Hao J, Li B, Li X, et al. An in-depth study of Zn metal surface chemistry for advanced aqueous Zn-ion batteries. *Adv Mater.* 2020;32:2003021.
6. Wang D, Liu H, Lv D, Wang C, Yang J, Qian Y. Rational screening of artificial solid electrolyte interphases on Zn for ultrahigh-rate and long-life aqueous batteries. *Adv Mater.* 2023;35:2207908.
7. Luo B, Wang Y, Zheng S, et al. Ion pumping synergy with atomic anchoring for dendrite-free Zn anodes. *Energy Storage Mater.* 2022;51:610-619.
8. Wang D, Lv D, Peng H, et al. Site-selective adsorption on ZnF_2/Ag coated Zn for advanced aqueous zinc-metal batteries at low temperature. *Nano Lett.* 2022;22:1750-1758.
9. Wang Y, Guo T, Yin J, et al. Controlled deposition of zinc-metal anodes via selectively polarized ferroelectric polymers. *Adv Mater.* 2022;34:2106937.
10. Zeng Y, Zhang X, Qin R, et al. Dendrite-free zinc deposition induced by multifunctional CNT frameworks for stable flexible Zn-ion batteries. *Adv Mater.* 2019;31:1903675.
11. Yang Q, Guo Y, Yan B, et al. Hydrogen-substituted graphdiyne ion tunnels directing concentration redistribution for commercial-grade dendrite-free zinc anodes. *Adv Mater.* 2020;32:2001755.
12. Verma V, Kumar S, Manalastas W, Satish R, Srinivasan M. Progress in rechargeable aqueouszinc- and aluminum-ion battery electrodes: Challenges and outlook. *Adv Sustain Syst.* 2019;3:1800111.
13. Liu P, Zhang Z, Hao R, et al. Ultra-highly stable zinc metal anode via 3D-printed g-C_3N_4 modulating interface for long life energy storage systems. *Chem Eng J.* 2021;403:126425.
14. Wu K, Cui J, Yi J, et al. Biodegradable gel electrolyte suppressing water-induced issues for long-life zinc metal anodes. *ACS Appl Mater Interfaces.* 2022;14:34612-34619.
15. Zhang B, Qin L, Fang Y, et al. Tuning Zn^{2+} coordination tunnel by hierarchical gel electrolyte for dendrite-free zinc anode. *Science Bulletin.* 2022;67:955-962.

16. Gou Q, Luo H, Zhang Q, et al. Electrolyte regulation of bio-inspired zincophilic additive toward high-performance dendrite-free aqueous zinc-ion batteries. *Small.* 2023;19: 2207502.

17. Hou Z, Gao Y, Tan H, Zhang B. Realizing high-power and high-capacity zinc/sodium metal anodes through interfacial chemistry regulation. *Nat Commun.* 2021;12:3083.

18. Li Q, Yan B, Wang D, et al. Mechanistic study of interfacial modification for stable Zn anode based on a thin separator. *Small.* 2022;18:2201045.

19. An Y, Tian Y, Liu C, Xiong S, Feng J, Qian Y. Rational design of sulfur-doped three-dimensional $Ti_3C_2T_x$ Mxene/ZnS heterostructure as multifunctional protective layer for dendrite-free zinc-ion batteries. *ACS Nano.* 2021;15:15259-15273.

20. Han J, Euchner H, Kuenzel M, et al. A thin and uniform fluoride-based artificial interphase for the zinc metal anode enabling reversible Zn/MnO_2 batteries. *ACS Energy Lett.* 2021;6:3063-3071.

21. He H, Qin H, Wu J, et al. Engineering interfacial layers to enable Zn metal anodes for aqueous zinc-ion batteries. *Energy Storage Mater.* 2021;43:317-336.

22. Kang L, Cui M, Jiang F, et al. Nanoporous $CaCO_3$ coatings enabled uniform Zn stripping/plating for long-life zinc rechargeable aqueous batteries. *Adv Energy Mater.* 2018;8: 1801090.

23. Liu M, Yang L, Liu H, et al. Artificial solid-electrolyte interface facilitating dendrite-free zinc metal anodes via nanowetting effect. *ACS Appl Mater Interfaces.* 2019;11:32046-32051.

24. Liu X, Yang F, Xu W, Zeng Y, He J, Lu X. Zeolitic imidazolate frameworks as Zn^{2+} modulation layers to enable dendrite-free Zn anodes. *Adv Sci.* 2020;7:2002173.

25. Lu Q, Liu C, Du Y, et al. Uniform Zn deposition achieved by Ag coating for improved aqueous zinc-ion batteries. *ACS Appl Mater Interfaces.* 2021;13:16869-16875.

26. Yang X, Li C, Sun Z, et al. Interfacial manipulation via in situ grown ZnSe cultivator toward highly reversible Zn metal anodes. *Adv Mater.* 2021;33:2105951.

27. Tao F, Liu Y, Ren X, et al. Different surface modification methods and coating materials of zinc metal anode. *J Energy Chem.* 2022;66:397-412.

28. Hao J, Li X, Zhang S, et al. Designing dendrite-free zinc anodes for advanced aqueous zinc batteries. *Adv Funct Mater.* 2020;30:2001263.

29. Wang SB, Ran Q, Yao RQ, et al. Lamella-nanostructured eutectic zinc-aluminum alloys as reversible and dendrite-free anodes for aqueous rechargeable batteries. *Nat Commun.* 2020;11:1634.

30. Yan H, Li S, Nan Y, Yang S, Li B. Ultrafast zinc-ion-conductor interface toward high-rate and stable zinc metal batteries. *Adv Energy Mater.* 2021;11:2100186.

31. Yuksel R, Buyukcakir O, Seong WK, Ruoff RS. Metal-organic framework integrated anodes for aqueous zinc-ion batteries. *Adv Energy Mater.* 2020;10:1904215.

32. Ren J, Li C, Li P, Liu S, Wang L. Amorphous MOF as smart artificial solid/electrolyte interphase for highly-stable Zn-ion batteries. *Chem Eng J.* 2023;462:142270.

33. Yang H, Chang Z, Qiao Y, et al. Constructing a super-saturated electrolyte front surface for stable rechargeable aqueous zinc batteries. *Angew Chem.* 2020;132:9463-9467.

34. Li B, Xue J, Han C, et al. A hafnium oxide-coated dendrite-free zinc anode for rechargeable aqueous zinc-ion batteries. *J Colloid Interface Sci.* 2021;599:467-475.

35. Zhao RR, Yang Y, Liu GX, et al. Redirected Zn electrodeposition by an anti-corrosion elastic constraint for highly reversible Zn anodes. *Adv Funct Mater.* 2020;31:2001867.

36. Yan Z, Xin W, Zhu Z. Artificial interphase engineering to stabilize aqueous zinc metal anodes. *Nanoscale.* 2021;13: 19828-19839.

37. Hong L, Wang LY, Wang Y, et al. Toward hydrogen-free and dendrite-free aqueous zinc batteries: formation of zincophilic protective layer on Zn anodes. *Adv Sci.* 2022;9:2104866.

38. Li Y, Yang S, Du H, et al. A stable fluoride-based interphase for a long cycle Zn metal anode in an aqueous zinc ion battery. *J Mater Chem A.* 2022;10:14399-14410.

39. Fang G, Zhou J, Pan A, Liang S. Recent advances in aqueous zinc-ion batteries. *ACS Energy Lett.* 2018;3:2480-2501.

40. Xin W, Xiao J, Li J, et al. Metal-organic frameworks with carboxyl functionalized channels as multifunctional ion-conductive interphase for highly reversible Zn anode. *Energy Storage Mater.* 2023;56:76-86.

41. Wang R, Xin S, Chao D, et al. Fast and regulated zinc deposition in a semiconductor substrate toward high-performance aqueous rechargeable batteries. *Adv Funct Mater.* 2022;32:2207751.

42. Xie X, Liang S, Gao J, et al. Manipulating the ion-transfer kinetics and interface stability for high-performance zinc metal anodes. *Energy Environ Sci.* 2020;13:503-510.

43. Cao P, Zhou X, Wei A, et al. Fast-charging and ultrahigh-capacity zinc metal anode for high-performance aqueous zinc-ion batteries. *Adv Funct Mater.* 2021;31:2100398.

44. Yang J, Yin B, Sun Y, et al. Zinc anode for mild aqueous Zinc-Ion batteries: challenges, strategies, and perspectives. *Nanomicro Lett.* 2022;14:42.

45. Wang T, Xi Q, Li Y, et al. Regulating dendrite-free zinc deposition by red phosphorous-derived artificial protective layer for zinc metal batteries. *Adv Sci.* 2022;9:2200155.

46. Liu Y, Liu Y, Wu X. Toward long-life aqueous zinc ion batteries by constructing stable zinc anodes. *Chem Rec.* 2022; 22:e202200088.

47. Nam K-H, Hwa Y, Park C-M. Zinc phosphides as outstanding sodium-ion battery anodes. *ACS Appl Mater Interfaces.* 2020; 12:15053-15062.

48. Zheng J, Huang Z, Ming F, et al. Surface and interface engineering of Zn anodes in aqueous rechargeable Zn-ion batteries. *Small.* 2022;18:2200006.

49. Hu L, Xiao P, Xue L, Li H, Zhai T. The rising zinc anodes for high-energy aqueous batteries. *EnergyChem.* 2021;3: 100052.

50. Deng C, Xie X, Han J, Lu B, Liang S, Zhou J. Stabilization of Zn metal anode through surface reconstruction of a cerium-based conversion film. *Adv Funct Mater.* 2021;31:2103227.

51. Cao Z, Zhu X, Xu D, et al. Eliminating Zn dendrites by commercial cyanoacrylate adhesive for zinc ion battery. *Energy Storage Mater.* 2021;36:132-138.

52. Yuan C, Yin L, Du P, et al. Microgroove-patterned Zn metal anode enables ultra-stable and low-overpotential Zn deposition for long-cycling aqueous batteries. *Chem Eng J.* 2022;442:136231.

53. Guo C, Zhou J, Chen Y, et al. Integrated micro space electrostatic field in aqueous Zn-ion battery: scalable electrospray fabrication of porous crystalline anode coating. *Angew Chem Int Ed*. 2023;62:e202300125.

54. Chen P, Yuan X, Xia Y, et al. An artificial polyacrylonitrile coating layer confining zinc dendrite growth for highly reversible aqueous zinc-based batteries. *Adv Sci*. 2021;8:2100309.

55. Li Q, Zhao Y, Mo F, et al. Dendrites issues and advances in Zn anode for aqueous rechargeable Zn-based batteries. *EcoMat*. 2020;2:e12035.

56. Xie C, Li Y, Wang Q, Sun D, Tang Y, Wang H. Issues and solutions toward zinc anode in aqueous zinc-ion batteries: a mini review. *Carbon Energy*. 2020;2:540-560.

SUPPORTING INFORMATION

Additional supporting information can be found online in the Supporting Information section at the end of this article.